



LAWRENCE
LIVERMORE
NATIONAL
LABORATORY

High-Energy X-Ray Imager for Laser-Fusion Research at the National Ignition Facility

R. Tommasini, J. Koch

April 25, 2005

Disclaimer

This document was prepared as an account of work sponsored by an agency of the United States Government. Neither the United States Government nor the University of California nor any of their employees, makes any warranty, express or implied, or assumes any legal liability or responsibility for the accuracy, completeness, or usefulness of any information, apparatus, product, or process disclosed, or represents that its use would not infringe privately owned rights. Reference herein to any specific commercial product, process, or service by trade name, trademark, manufacturer, or otherwise, does not necessarily constitute or imply its endorsement, recommendation, or favoring by the United States Government or the University of California. The views and opinions of authors expressed herein do not necessarily state or reflect those of the United States Government or the University of California, and shall not be used for advertising or product endorsement purposes.

This work was performed under the auspices of the U.S. Department of Energy by University of California, Lawrence Livermore National Laboratory under Contract W-7405-Eng-48.

High-Energy X-Ray Imager for laser-fusion research at the National Ignition Facility

Riccardo Tommasini, Jeff Koch

Summary

X-ray imaging will be an important diagnostic tool for inertial confinement fusion (ICF) research at the National Ignition Facility (NIF). However, high neutron yields will make x-ray imaging much more difficult than it is at smaller facilities.

We analyze the feasibility and performance of a High-Energy X-Ray Imager (HEXRI) to be used on cryogenic DT implosions at NIF, with particular emphasis on spatial-resolution, field of view, signal-to-background and signal-to-noise ratios. Using a pinhole about 4 μm in diameter a resolution of 5.8 μm is achieved at 9 keV, limited by restrictions in the pinhole positioning. The resolution varies between 8.5 and 4.5 μm in the 5 - 20 keV spectral range.

Different options for the scintillating materials have been evaluated with the goal of having a sufficiently fast phosphor screen to allow time gating for minimizing neutron-induced background.

Signal/Background (SBR) and Signal/Noise (SNR) ratios (limited to x-rays) have been calculated for different commercially-available scintillators, both showing adequate values with either a tantalum or a platinum pinhole substrate.

Introduction

The HEXRI system is intended to provide time-integrated, broadband, moderate-energy x-ray core images of imploding ICF capsules. Highly magnified, spectrally-filtered images created using an array of pinholes placed close to the target will be projected onto a scintillator placed at the target chamber wall. Filters placed in front of the scintillator will restrict the x-ray spectrum transmitted to the phosphor screen. A telescope will be used to relay the scintillator emission to a distant detector that is time-gated in order to minimize backgrounds, in particular from neutrons. To summarize, the primary requirements for such a system are:

- Imaging spectral range around 5-20 keV
- Field of view: larger than 100 μm at the target plane
- Spatial resolution: about 5 μm at 9keV
- Time gating to eliminate neutron background (expected to be up to 10^{19} total yield)
- Adequate signal-to-noise and signal-to-background ratios
- A minimum of 10×10 array of images, differentially filtered in order to obtain hot-spot temperature and density maps.

Concept

A diagram of the simplified set up is shown in Figure 1, together with the definitions of the main parameters.

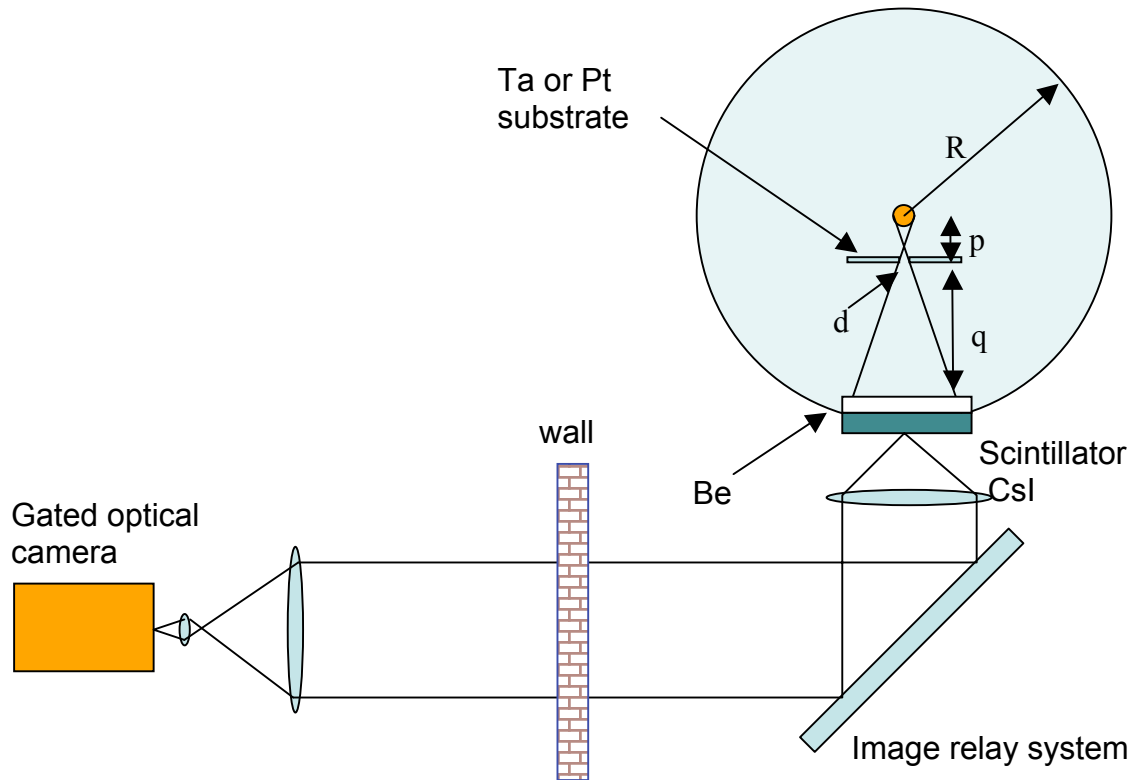


Figure 1: Sketch of the simplified set up for the Ignition X-Ray Imager

The source characteristics are estimated from 1-D simulations. In particular here we assume the peak brightness for the igniting core to be $B_0=10^{16}$ W / (cm² Sr keV) at 9 keV, with a duration $\Delta t \sim 100$ ps. [Ref.1]

Neutron Background and Detection system

The emitted neutron distribution is expected to peak at 14 MeV, meaning that the neutrons from the implosions will need 100 ns to cover the 5 m radial distance from the TC center to the scintillator or TC walls. Therefore, in principle, we can eliminate the neutron background by time gating, provided that both the gated optical detector window and the scintillator have decay times shorter than ~ 50 ns. A pure CsI scintillator fits this requirement,

having a decay time of about 16 ns, with a conversion efficiency of 2 ph/keV [Ref.2]. Possible alternatives include: CsF [Ref.2], with a shorter decay time, 5 ns, and same efficiency; Yttrium Aluminum Perovskite (YAP:Ce), with a decay time of about 25 ns and an efficiency of 18 ph/keV [Ref.2, 3]; and BaF [Ref.2], with an extremely short decay time, 0.6 ns (fast component), and an efficiency of 1.8 ph/keV. The main characteristics of these phosphors are reported in Table 1.

Material	Yield (ph/keV)	Decay time (ns)	Refractive index at peak emission	λ emission (nm)
CsF	2	5	1.95	390
CsI	2	16	1.48	310
YAP:Ce	18	25	1.94	350
BaF	1.8 (fast)	0.6 (fast)	1.54	220 (fast)

Table 1: Main parameters of the scintillators investigated [Ref. 2]

However the background from neutrons as well as gamma rays from neutron-gamma reactions represents a complex issue for the proposed set up and needs more careful consideration. We are currently studying the issue using a Monte Carlo code, and will report the results at a later time.

Pinhole camera resolution

The spatial resolution σ on the object plane of a pinhole camera is assumed to be the convolution of the geometrical resolution and the diffraction point spread function [Ref.4]:

$$\sigma^2 = \sigma_{geom}^2 + \sigma_{diff}^2$$

$$\sigma_{geom} = d(p + q) / q = d \frac{M + 1}{M} \tag{Eq. 1}$$

$$\sigma_{diff} = \frac{2.44\lambda p}{d}$$

Being d the diameter of the pinhole, p the object-to-pinhole distance, q the pinhole-to-detector distance, λ the wavelength and $M=q/p$ the magnification. The optimal pinhole diameter is found minimizing σ :

$$\frac{\partial \sigma}{\partial d} = 0; \Rightarrow d_{\text{opt}} = \sqrt{\frac{2.44 p \lambda M}{M+1}} \quad \text{Eq. 2}$$

Substituting this value back into the equation for σ , we get:

$$p = \frac{M \sigma^2}{4.88 \lambda (M+1)} \quad \text{Eq. 3}$$

$$d_{\text{opt}} = \frac{M \sigma}{\sqrt{2(M+1)}}$$

Notice that for the above values of d and p the diffraction and geometric part of the spatial resolution are equalized being each equal to $\sigma^2/2$, so that

$$\sigma^2 = 2 \left(\frac{2.44 \lambda p}{d} \right)^2 = 2 \left(\frac{(M+1)d}{M} \right)^2 \quad \text{Eq. 4}$$

Obviously the resolution can be optimized for a single wavelength only. Since we want the scintillator on the TC wall, we require $p+q=R$, being R the TC radius. Therefore we have to fulfill the condition $p(1+M) = R$ giving:

$$M = \frac{4.88 \lambda R}{\sigma^2}; \quad p = \frac{R}{1 + \frac{4.88 \lambda R}{\sigma^2}}; \quad d_{\text{opt}} = \frac{4.88 \lambda R \sigma}{\sqrt{2(4.88 \lambda R + \sigma^2)}} \quad \text{Eq. 5}$$

Pinhole camera geometry				
	p+q [m]	σ (μm)	E (keV)	λ (nm)
Fixed Parameters	5.0	5.0	9.0	0.14
calculated parameters		7.3	5.0	0.25
		3.9	20.0	0.06
	M	p (mm)	d (μm)	q(mm)
	134	36.9	3.5	4963.1

Table 2: Pinhole camera parameters giving a resolution of 5 μm at 9 keV.

The above equations are useful in the case we are free to choose a resolution for a given wavelength. Table 2 shows the various values of the parameters, having chosen a resolution of 5 μm at 9 keV. The equation for M shows that at a fixed magnification, the resolution grows with the square root of the wavelength, as shown in the column “ σ ” of Table 2.

Figure 2 shows the behavior of the resolution at the various wavelengths vs. d , given the values of the parameters reported in Table 2, i.e. for achieving a nominal resolution of 5 μm at 9 keV.

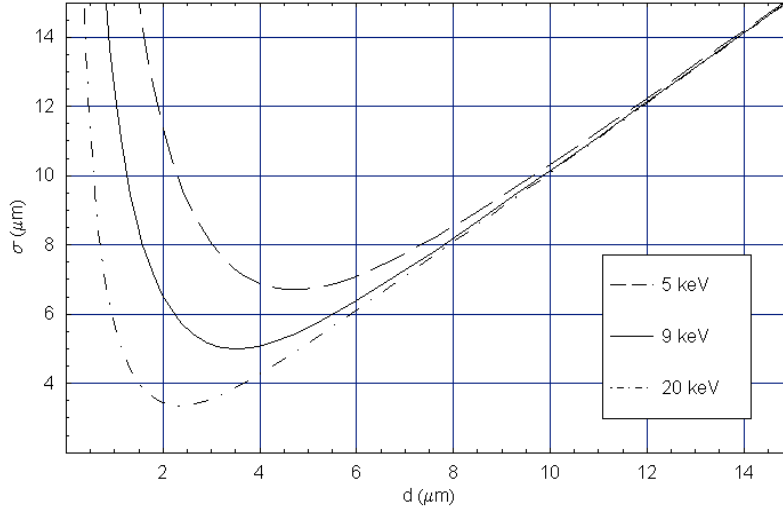


Figure 2: behavior of the resolution at the various wavelengths vs. d, given the values of the parameters reported in Table 2.

However for practical reasons the real constraint will be the minimum pinhole-source distance, which will be very likely limited to about 50 mm. When this is the case this condition will fix the resolution at the various wavelengths and the other parameters according to the equations:

$$M = \frac{R}{p} - 1; \quad \sigma = \sqrt{\frac{4.88 p \lambda}{1 - p/R}}; \quad d_{opt} = \sqrt{2.44 p \lambda (1 - p/R)} \quad \text{Eq. 6}$$

Since $R \gg p$, the above relations assume a particularly simple form:

$$M \cong \frac{R}{p}; \quad \sigma \cong \sqrt{4.88 p \lambda}; \quad d_{opt} \cong \sqrt{2.44 p \lambda} \quad \text{Eq. 7}$$

Pinhole camera geometry				
	p+q [m]	p (mm)		
Fixed Parameters	5.0	50.0		
calculated parameters	M	$\sigma(\mu\text{m})$	E (keV)	λ (nm)
	99	5.8	9.0	0.14
		8.5	5.0	0.25
		4.5	20.0	0.06
			d (μm)	q(mm)
			4.1	4950.0

Table 3: Pinhole camera parameters for a minimum distance from target of 50 mm.

The results are shown in Table 3. We see that the above condition limits the resolution at 9 keV to 5.8 μm . Figure 3 shows the resolution vs. x-ray energy for both cases examined here: free choice of pinhole-to-source distance (dashed line) and pinhole-to-source distance fixed to 50mm (solid line).

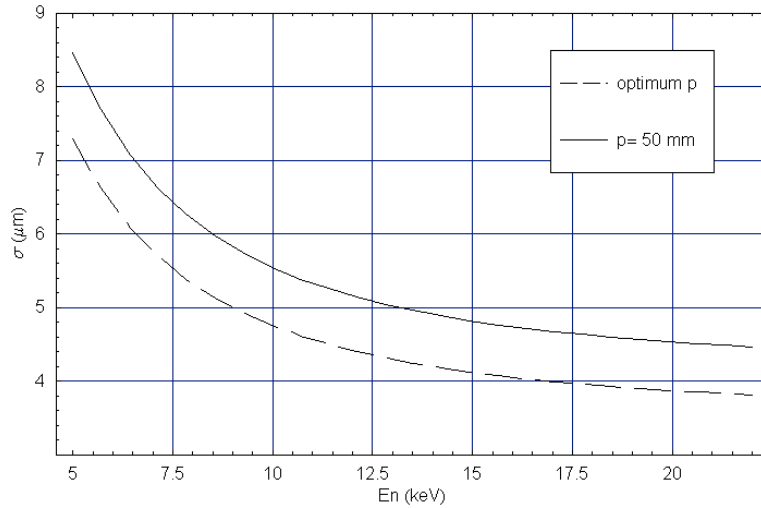


Figure 3: resolution vs. x-ray energy for both cases examined here: free choice of pinhole-to-source distance (dashed) and pinhole-to-source distance fixed to 50mm (solid line).

Field Of View

The field of view (FOV) can be limited by the thickness t_{ph} of the pinhole substrate or by the detector area. From simple geometry we find that $t_{ph} = 2 \frac{pd}{FOV}$. Given the parameters of Table 3, and assuming a minimum FOV of 100 μm , we find a maximum allowable value for the thickness of 11.6 mm. The pinhole thickness is therefore never a concern for the FOV, which is in turn limited only by the detector size.

Scintillator

For a given x-ray energy spectrum, the scintillator performance is a strong function of its thickness. The x-ray absorption efficiency increases with scintillator thickness, while the primary sources of image blur (radiation scattering in the scintillator and depth-of-focus of the optical system) increase linearly with the scintillator thickness. As a result designing a system for which

spatial resolution is the driving concern favors a relatively thin converter; conversely, designing a system in which statistical detection is of paramount importance favors a thicker converter. We note that a thin converter also minimizes the background, e.g. from gamma rays which need large thicknesses to be efficiently absorbed.

Depth-of-focus blurring

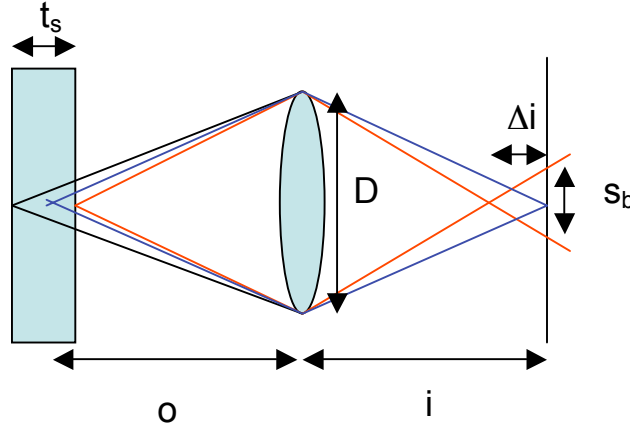


Figure 4: sketch illustrating depth-of-focus blurring.

With reference to Figure 4, where a general optical system is assumed to image the scintillator over a CCD camera, we calculate the image point shift Δi , corresponding to a scintillator thickness t_s . Differentiating the thin lens equation we get:

$$\frac{1}{i} + \frac{1}{o} = \frac{1}{f} \Rightarrow \frac{\Delta i}{i^2} + \frac{\Delta o}{o^2} = 0 \Rightarrow \frac{\Delta i}{i} = -\frac{t_s}{2o} M_i \quad \text{Eq. 8}$$

Where M_i is the magnification of the imaging system. Simple geometry gives:

$$s_b = \frac{D}{i - \Delta i} \Delta i = \frac{D \frac{t_s}{2}}{\frac{o}{M_i} + \frac{t_s}{2}} \sim D \frac{t_s}{2} \frac{M_i}{o} \quad \text{Eq. 9}$$

Notice that according to the set up shown in Figure 1, o is simply the focal length and Eq.9 can be rewritten as:

$$s_b = \frac{t_s}{2} \frac{M_i}{F} \quad \text{Eq. 10}$$

Where F is the lens f-number. It follows that s_b can be mitigated by choosing a small enough magnification and/or scintillator thickness or a relatively large f-number.

Radiation-scattering blurring

Regarding the blurring due to radiation scattering, this is easily estimated to be linear with the scintillator thickness. A good rule of thumb is to assume the resolution to be twice the thickness:

$$s_s \sim 2t_s \tag{Eq. 11}$$

As a consequence this effect can be minimized only by reducing the scintillator thickness or by using a scintillator grown in columns to simultaneously enhance the radiation absorption (i.e. large values of t_s) and the spatial resolution, in this case limited by the diameter of the scintillating columns (or fibers).

Upper Limit for the Scintillator thickness

Given an intrinsic scintillator resolution s , the total resolution on the source plane is $\sigma_t^2 = \sigma^2 + (s/M)^2 = \sigma^2(1 + s^2/(\sigma M)^2)$. We therefore require $s \ll M\sigma$. Defining $s = m\sigma$ and assuming $M \sim 100$, we get $\sigma_t \sim \sigma(1 + (m/M)^2/2)$, admitting a maximum blurring of 3%, we require $(m/M)^2 = 3/50$. Hence $s \leq 24 \sigma \sim 140 \mu\text{m}$, for a resolution of $5.8 \mu\text{m}$. The thickness limit for the scintillator is thus $70 \mu\text{m}$. Notice however that the absorption efficiency does not vary significantly. For example, for CsI at 9 keV, the absorption is 0.999 and 0.912 for 70 and 25 μm thicknesses, respectively, which would correspond, in first approximation, to an improvement of about $(0.999/0.912)^{1/2} - 1 = 5 \%$ in SNR. Hence a 25 μm baseline for the scintillator thickness seems perfectly adequate and corresponds to $s = 50 \mu\text{m}$.

Image Relay Optics

The scintillator is imaged over a CCD through an image relay system. The CCD image plane corresponds to a particular object plane of the scintillator. The regions of the scintillator out of this plane create a blurred image on the CCD. This situation has been analyzed in the previous section (depth of focus blurring). On the scintillator plane, the depth of focus blurring is simply (see Eq. 10)

$$\sigma_{df} \sim \frac{t_s}{2F} \quad \text{Eq. 12}$$

The combined resolution of the system is obtained convolving to this term the contribution of radiation scattering and of diffraction from the telescope aperture. Hence we have:

$$\sigma_{sp}^2 = \left(D \frac{t_s}{2f}\right)^2 + \left(2.44 \frac{\lambda f}{D}\right)^2 + at_s^2 = \left(a \frac{t_s}{F}\right)^2 + (b\lambda F)^2 + (ct_s)^2 \quad \text{Eq. 13}$$

where F is the imaging system F number. We also generalized the various coefficients: $a = 0.5$, $b = 2.44$, $c \sim 2$. We optimize the resolution minimizing σ_{IR} vs. F.

$$\frac{\partial \sigma_{sp}}{\partial F} = 0; \Rightarrow F_{opt} = \sqrt{\frac{at_s}{b\lambda}} \quad \text{Eq. 14}$$

The optimum thickness is found substituting the value of F_{opt} back into Eq.13 and solving for t_s , giving:

$$t_{s,opt} = \frac{\sqrt{a^2 b^2 \lambda^2 + c^2 \sigma_{sp}^2} - ab\lambda}{c^2} \quad \text{Eq. 15}$$

While in principle it is possible to choose an optimum F number to maximize the resolution at the scintillator plane, it is easy to realize that in our case, given the values of the parameters a, b and c, Eq.13 is dominated by the last term, so that any dependency on F is marginal. Using our current parameters, a resolution at the scintillator plane of $50 \mu\text{m}$ and an emitting wavelength for the scintillator of 310 nm , we get $t_{opt} = 24.9 \mu\text{m}$, which is very close to the $25 \mu\text{m}$ of choice. Figure 5 shows the variation of σ_{sp} vs. F-number. As seen, while an optimum value exists at about 4, variations of the F number in the range 1-15 do not change significantly the value of σ_{sp} .

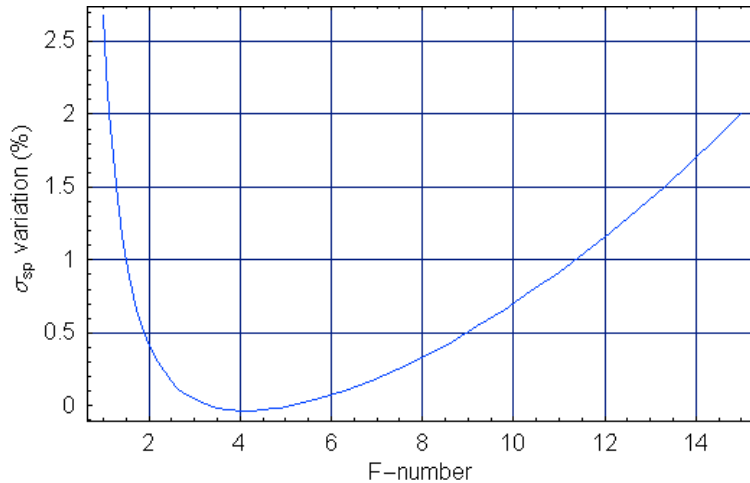


Figure 5: variation (%) of the resolution at scintillator plane, σ_{sp} , vs. F-number.

Photometrics

Having characterized the various components of the system we now calculate the scintillator output, the background and the signal-to-noise ratio, per single image.

Incident Photons per resolution element and X-ray background

We assume a source with brightness B_0 , where $[B_0] = J / (cm^2 Sr keV)$. The image brightness B_I from a pinhole is easily found to be:

$$B_{I[J/cm^2SrkeV]} = B_{0[J/(cm^2SrkeV)]} \frac{\Omega}{M^2} \quad \text{Eq. 16}$$

Where $\Omega = \pi (d/2)^2 / p^2$ is the solid angle subtended by the pinhole. Introducing the time duration of the source, Δt , and an overall transmission coefficient T , we get:

$$B_{I[J/cm^2SrkeV]} = B_{0[W/(cm^2SrkeV)]} \frac{\Omega}{M^2} T \Delta t \quad \text{Eq. 17}$$

Where we have changed the units of B_0 accordingly. The source spectrum has been estimated from 1-D simulations [Ref.1]. In particular a Bremsstrahlung profile, corresponding to a temperature of 5keV, has been rescaled in order to have a peak brightness for the igniting core of $10^{16} W / (cm^2 Sr keV)$ at 9 keV. The brightness of the radiation impinging on the phosphor screen has been calculated considering a 10 μm thick Au hohlraum and a 7mm-thick Be filter in front of the scintillator, with a duration $\Delta t \sim 100$ ps for the X-ray burst. Defining I_0 the photon emissivity of the source, where $[I_0] = (\text{Number of Photons}) / (cm^2 Sr)$, the number of photons per resolution element arriving on the detector is:

$$N_{[photons/res.element]} = I_0 \frac{\pi(\sigma/2)^2 \pi(d/2)^2}{p^2} = I_0 \frac{\pi^2 \sigma^2 d^2}{16p^2} \quad \text{Eq. 18}$$

It is worth noticing that I_0 depends on the wavelength. If we define the optimized wavelength to be the one for which we decide to optimize the resolution, then we can use Eq. 4 and the number of photons per resolution element at the optimized wavelength assumes two very simple forms, the second of which explicitly shows a dependence on the wavelength only:

$$N_{[\text{photons/res.element}]}(\lambda_{opt}) = I_0 \left(\pi \frac{(M+1)d^2}{Mp} \right)^2 = I_0 \frac{(2.44)^2 \pi^2}{8} \lambda^2 \quad \text{Eq. 19}$$

A different and more interesting way to recover this result is as follows. Substituting Eq. 1 into Eq. 19 we get

$$N_{[\text{photons/res.element}]} = I_0 \frac{\pi^2}{16} \left(\frac{d^4}{p^2} \left(\frac{M+1}{M} \right)^2 + 2.44^2 \lambda^2 \right) \quad \text{Eq. 20}$$

where the first term in brackets is due to the geometry and the second to diffraction. Since optimizing the resolution implies equating the two contributions, we have:

$$N_{[\text{photons/res.element}]}(\lambda_{opt}) = 2I_0 \frac{\pi^2}{16} (2.44^2 \lambda^2) \quad \text{Eq. 21}$$

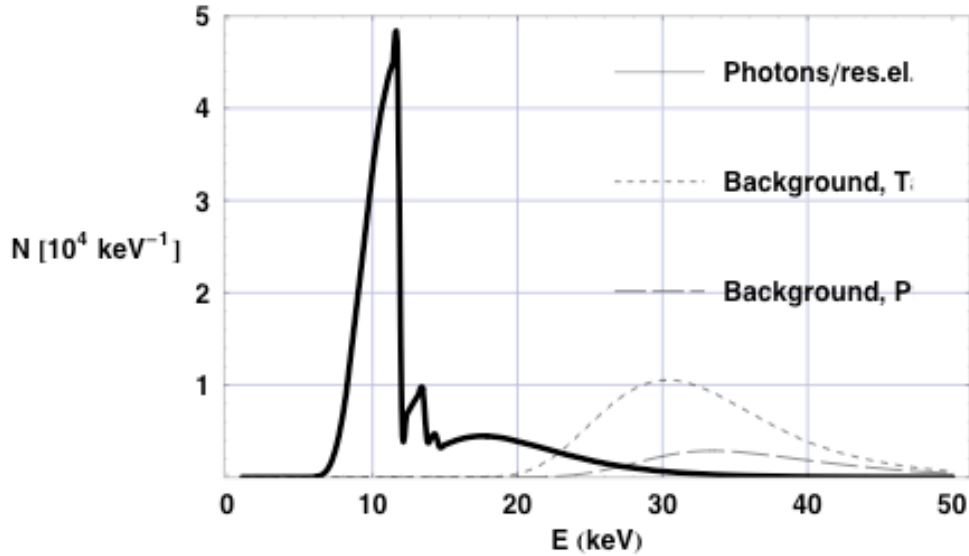


Figure 6: Number of photons per resolution element impinging on the detector (solid line); Background from X-rays directly traversing the pinhole substrate (dashed lines).

Figure 6 (solid line) shows the calculated number of photons per resolution element vs. photon energy. Background is generated by x-rays passing through the pinhole substrate around the aperture. In this case the thickness and composition of the substrate can be of concern. For our

calculations we assumed a reasonably large, but still feasible, thickness of 75 μm for the pinhole substrate. The dashed lines of Figure 6 show the background signal for a 75mm-thick Ta and Pt substrate, assuming the source to have a diameter of 60 μm . The difference is mainly due to the higher density of Pt (21.45 g/cm^3) with respect to Ta (16.654 g/cm^3).

Scintillator Signal and Background

To calculate the output from the various phosphor screens listed in Table 1, tabulated data for the linear absorption coefficient [Ref.5] have been fitted to cubic splines. Figure 7 reports the results of the procedure for the scintillators under consideration.

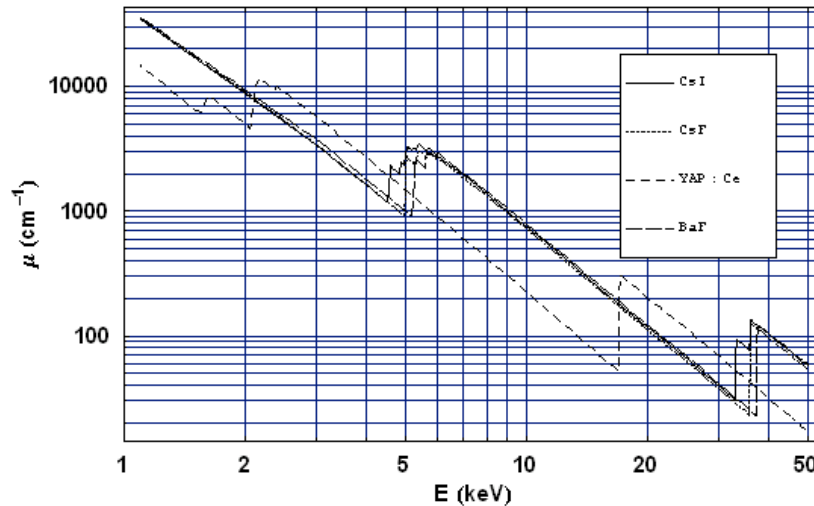


Figure 7: linear absorption coefficients for the scintillators under consideration

The phosphor screens output was calculated assuming 25 μm -thick scintillators having yield as reported in Table 1, and an absorption efficiency η , where $\eta = 1 - \exp(-\mu t_s)$, being μ the linear absorption coefficient As mentioned above, η is an increasing function of t_s , while the resolution decreases with increasing t_s .

Using the parameters reported in Table 3 we calculated the scintillators output N , i.e. number of photons per resolution element per unit bandwidth, as shown in Figure 8-11 (solid lines), together with the background using either a Ta or a Pt pinhole substrate.

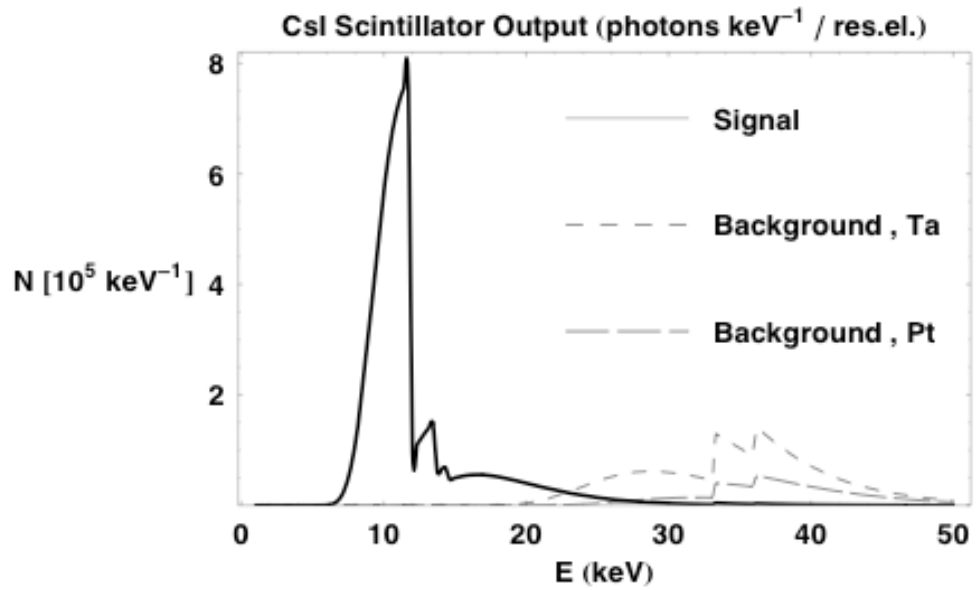


Figure 8: Predicted output signal for CsI

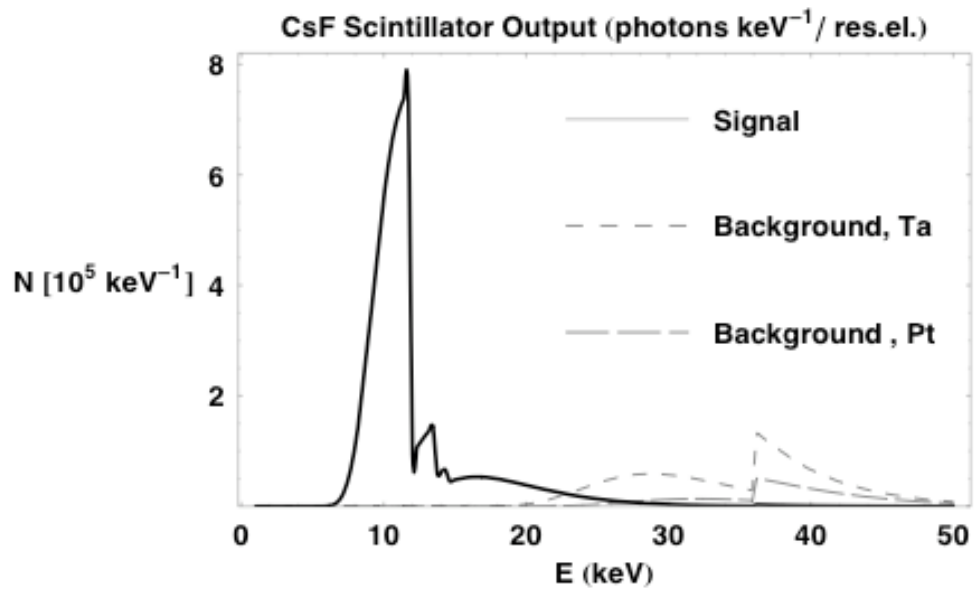


Figure 9: Predicted output signal for CsF

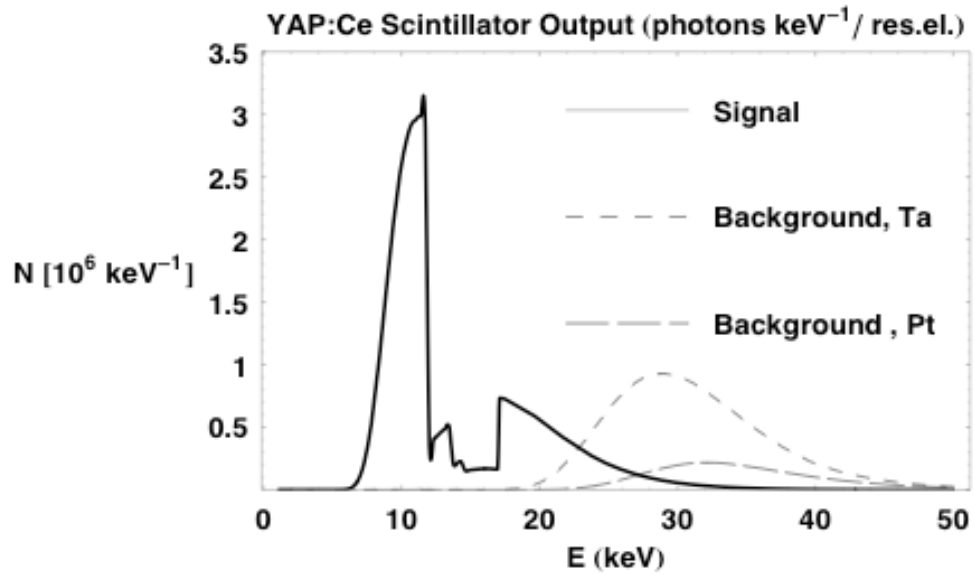


Figure 10: Predicted output signal for YAP:Ce

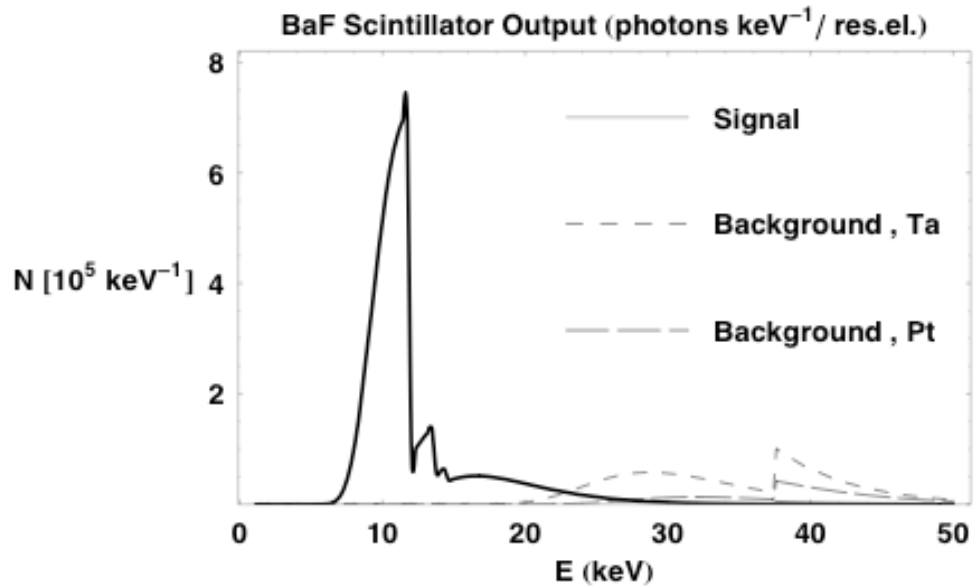


Figure 11: Predicted output signal for BaF

The respective values for the spectrally-integrated signal-to-background (SBR) are shown in Table 4.

Scintillator	SBR, Ta full spectrum	SBR, Pt full spectrum	SBR, Ta (1-30) keV	SBR, Pt (1-30) keV
CsI	2.0	6.3	7.6	61
CsF	2.5	7.6	7.8	63
YAP:Ce	1.5	5.8	2.8	22
BaF	2.6	8.6	7.5	60

Table 4: spectrally-integrated signal-to-background for the different phosphors

SNR

Assuming the detection processes to follow Poissonian statistics, the SNR at scintillator output is given by [Ref. 6]:

$$SNR_o^2 = N_0 \frac{\eta}{S^{-1} + n^{-1}} \quad \text{Eq. 22}$$

where N_0 is the number of incident photons, S is the Swank factor, n is the conversion efficiency, i.e. the number of visible photons emitted by the scintillator per incident x-ray. Using data from Swank, we find $S \sim 1$ to be a very good approximation for the various scintillators of different thicknesses and for incident x-ray energies below 50 keV, so that it is reasonable to simplify the above equation into

$$SNR_o^2 \sim N_0 \frac{\eta}{1 + n^{-1}} \quad \text{Eq. 23}$$

As mentioned above, η is an increasing function of t_s , while the resolution decreases with increasing t_s , so the choice of t_s is dictated by a compromise between the resolution and the SNR requirements.

The conversion efficiency for the scintillator is given by:

$$n_s = g\eta E_{avg} \quad \text{Eq. 25}$$

Where g is the scintillator efficiency (number of photons / keV) and E_{avg} is the average energy of the incident x-rays. Since the optical photons generated by the scintillator are transported to the CCD through the Image Relay System, in order to evaluate the SNR of the completed system we have to account for the conversion efficiency of the cascaded components [Ref. 7]:

$$n = \frac{n_s \cdot T_{IRS} \cdot n_{lc} \cdot QE_{CCD}}{k_s^2} \quad \text{Eq. 26}$$

Where T_{IRS} is the transmission of the image relay system, n_{lc} is the efficiency of the lens coupling, QE_{CCD} is the CCD quantum efficiency, κ_s is the scintillator refractive index at peak emission. The efficiency of lens coupling is simply given by the optical solid angle of the first lens of the imaging telescope:

$$n_{lc} = (4F)^{-2} \quad \text{Eq. 24}$$

Where F is the f-number of the optical system. Notice that n_{lc} decreases with increasing F . Due to the peak emissions falling into the UV spectral range, the optics will have to be fused Si. The transmission of the lenses to be used in the telescope is crucial to maintain high values of SNR.

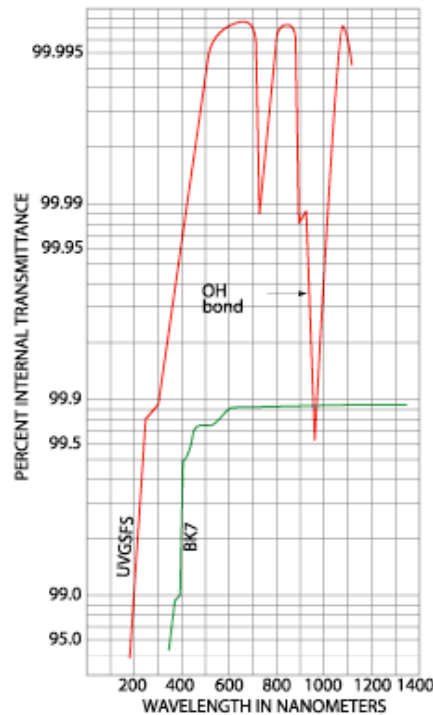


Figure 12: Semi logarithmic comparison of internal transmittances of UV-grade fused silica and BK7 glass (Melles Griot catalogue).

Figure 12 shows the internal transmission of UV-grade fused silica at different wavelengths. The values are high in the spectral region of interest, ranging from 99.0 at 200 nm up to 99.95 at 400 nm. Of particular interest is therefore having a good antireflection coating. Hebbbar coating [Ref.8] results in reflectances of less than 1% in the range 300-400nm, and around 2% at 220 nm.

In its final configuration the imaging system should produce a 10x10 array of images, differentially filtered to restrict their x-ray energy content in order to obtain hot-spot temperature and density maps. This together with the FOV minimum requirement of 100 μm and a magnification of about 100 for the pinhole camera, requires minimum scintillator dimensions on the order of about 15x15 cm. To image the phosphor screen over a typical CCD of 1-inch square frame size will require a telescope with demagnification $M_i \sim 1/7$.

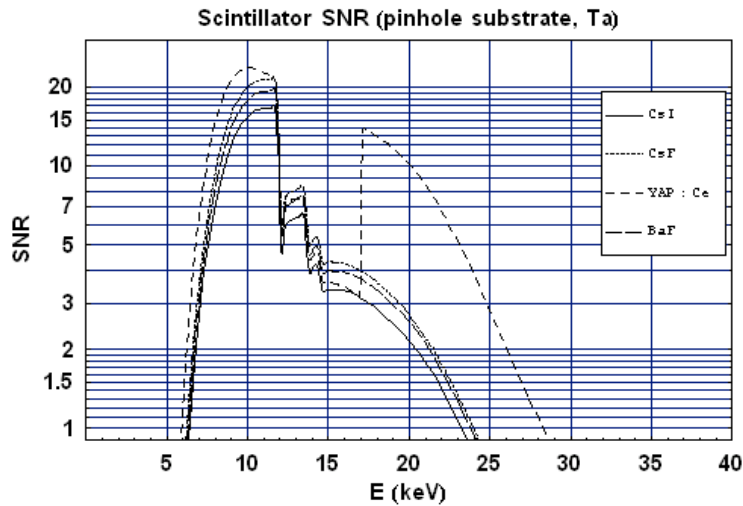


Figure 13: SNR of the cascaded detection system, assuming Ta as a pinhole substrate.

Figure 13 and 14 show the results for the SNR, including the noise from the background, of the cascaded detection system, assuming Ta and Pt as a pinhole substrate, respectively, for a value of 2 of the f-number and for the different scintillators.

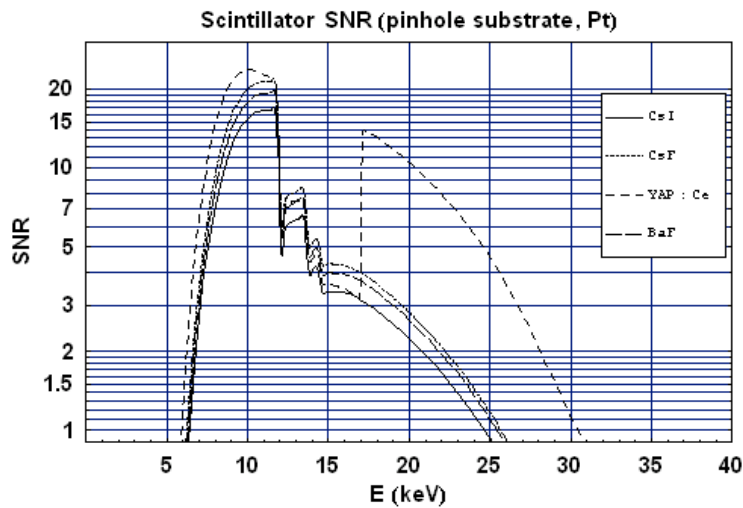


Figure 14: SNR of the cascaded detection system, assuming Pt as a pinhole substrate.

The main advantage of using Pt, in this case, is to extend the useful range of the SNR. Except at the lower end of the spectrum the SNR shows adequate values. In particular at 9keV the SNR is about the same for both substrates and attains the values shown in Table 5.

	CsI	CsF	YAP:Ce	BaF
SNR (@9keV)	12	15	21	14
SNR (@11keV)	16	21	22	19

Table 5: SNR at 9 keV and 11 keV for the four scintillators.

However the SNR has its maximum at about 11 keV, where the scintillator output reaches its peak. The corresponding values are shown in the second row of Table 5.

Figure 15 shows the spectrally integrated SNR and SBR, together with the loss (%) in resolution at the source plane, vs. scintillator thickness, using Pt as a pinhole substrate. As expected the SBR increases by reducing the thickness, since the absorption of high-energy photons is less efficient. The opposite is true for the SNR. We observe that the range of thickness between 25 and 50 μm shows the best compromise between SNR and SBR, except for YAP:Ce. Obviously the resolution is best for the minimum scintillator thickness.

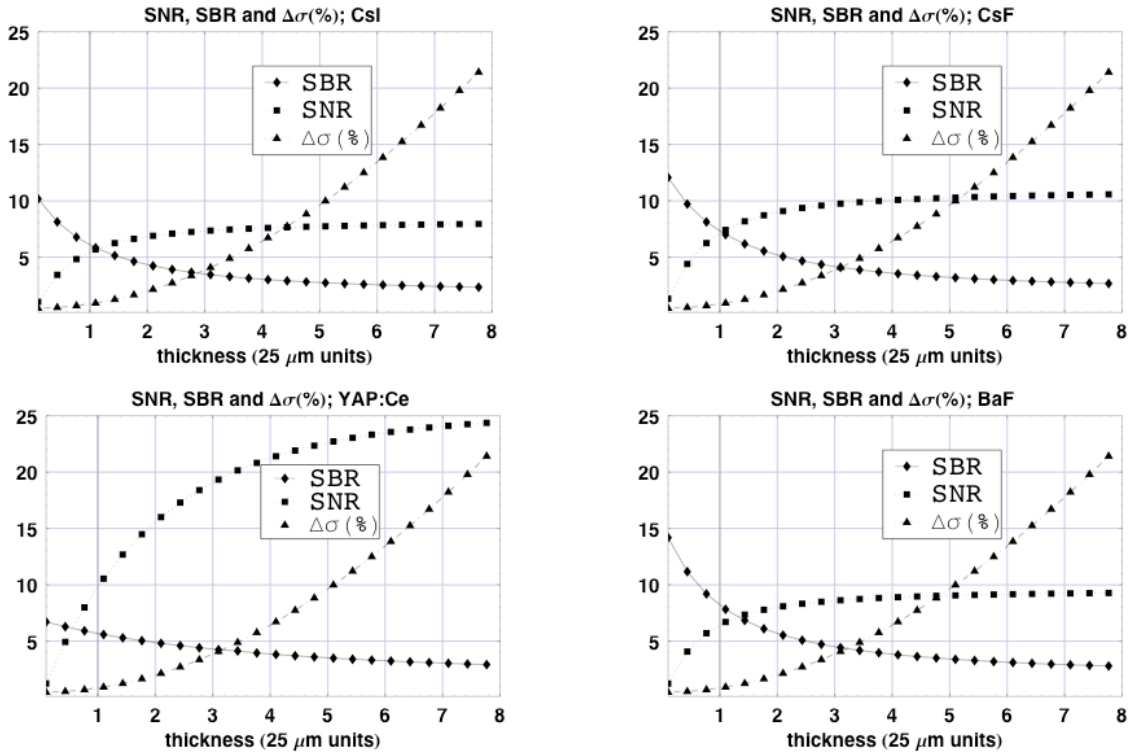


Figure 15: spectrally integrated SNR and SBR, together with the loss (%) in resolution at the source plane vs. scintillator thickness, using Pt as pinhole substrate

The SNR can be increased by using a reflection coating on the front side of the scintillator, thus restricting the emission of the scintillator over 2π (in place of 4π) with an improvement of a

factor of $\sqrt{2}$ in the SNR. The SNR can be further increased in the case the scintillator can be placed into the NIF target chamber thus allowing to use a much thinner Be filter. E.g. using a 1mm-thick Be filter results in an increase of about a factor of 1.5 for both the 9 keV and the spectrally-integrated values of the SNR.

Conclusions

An Ignition X-Ray Imager to be used on cryogenic DT implosions at NIF has been designed. Spatial-resolution at 9 keV is 5.8 μm accounting for limitations in the positioning the pinhole array. The system has a FOV adequate for a 10x10 array core images, differentially filtered in order to obtain hot-spot temperature and density maps. The SNR of the system is more than adequate, being well above 10 at 9 keV in most cases, and has margins for improvement. To summarize,

- Using a pinhole about 4 μm in diameter and various scintillators, 25 μm thick;
- A resolution 5.8 μm is achieved at 9 keV, limited by restrictions in the pinhole positioning. The resolution ranges between 8.5 and 4.5 μm in the 5-20 keV spectral range.
- Signal/Background (from x-rays) is adequate with either a Ta or a Pt substrate, with Pt showing a significant advantage.
- SNR (from statistics) is adequate in the range 6 – 20 keV, attaining values between 12 and 21 at 9 keV, for the different phosphors under evaluation.
- Substantial improvements in SNR are possible, with prospects to extend the detected spectral range, using a reflection coating on the front side of the scintillator and a thinner Be filter, in the case the scintillator can be placed into the NIF target chamber.

We are currently studying issues related to radiation damage of the scintillators and the effects of other sources of background, e.g. neutrons and gamma rays. The results will be reported in a future memo.

References

- [1] Steve Haan, private communication.
- [2] Saint Gobain, <http://www.detectors.saint-gobain.com>
- [3] M. Harada et al., Rev. Sci. Inst. 72 (11) 4308 (2001)
- [4] J. A. Koch et al., Appl. Opt. 37 (10) 1784 (1998)
- [5] NIST, National Institute of Standards and Technology, <http://physics.nist.gov>
- [6] Swank, J. Appl. Phys. 44, 4199 (1973)
- [7] Roehrig and Chen, SPIE Vol.2009, 144 (1993)
- [8] Melles Griot Catalogue